Shape-phase transitions in odd-mass gamma-soft nuclei with mass A ≈ 130

Nomura, Kosuke; Nikšić, Tamara; Vretenar, Dario

Shape-phase transitions in odd-mass γ-soft nuclei with mass $A \approx 130$

K. Nomura,[1,2] T. Nikšić,[1] and D. Vretenar[1]
[1]*Physics Department, Faculty of Science, University of Zagreb, 10000 Zagreb, Croatia*
[2]*Center for Computational Sciences, University of Tsukuba, Tsukuba 305-8577, Japan*
(Received 24 April 2017; published 7 July 2017)

Quantum phase transitions between competing equilibrium shapes of nuclei with an odd number of nucleons are explored using a microscopic framework of nuclear energy density functionals and a fermion-boson coupling model. The boson Hamiltonian for the even-even core nucleus, as well as the spherical single-particle energies and occupation probabilities of unpaired nucleons, are completely determined by a constrained self-consistent mean-field calculation for a specific choice of the energy density functional and pairing interaction. Only the strength parameters of the particle-core coupling have to be adjusted to reproduce a few empirical low-energy spectroscopic properties of the corresponding odd-mass system. The model is applied to the odd-A Ba, Xe, La, and Cs isotopes with mass $A \approx 130$, for which the corresponding even-even Ba and Xe nuclei present a typical case of γ-soft nuclear potential. The theoretical results reproduce the experimental low-energy excitation spectra and electromagnetic properties, and confirm that a phase transition between nearly spherical and γ-soft nuclear shapes occurs also in the odd-A systems.

DOI: 10.1103/PhysRevC.96.014304

I. INTRODUCTION

In many areas of physics and chemistry, quantum phase transitions (QPTs) present a prominent feature of strongly correlated many-body systems [1]. In atomic nuclei, in particular, a QPT occurs between competing ground-state shapes (spherical, axially deformed, and γ-soft shapes) as a function of a nonthermal control parameter—the nucleon number [2]. Even though in most cases nuclear shapes evolve gradually with nucleon number, in specific instances, with the addition or subtraction of only a few nucleons, a shape transition occurs characterized by a significant change of several observables and can be classified as a first-order or second-order QPT. Of course, in systems with a finite number of particles a QPT is smoothed out to a certain extent and, in the nuclear case, the physical control parameter takes on only integer values. Therefore, the essential issue in nuclear QPT concerns the identification of a particular nucleus at a critical point of phase transition, and the evaluation of observables that can be related to quantum order parameters.

Several empirical realizations of nuclear QPT and related critical-point phenomena have been observed in different regions of the chart of nuclides. In the rare-earth region, for instance, a rapid structural change occurs from spherical vibrational to axially deformed rotational nuclei, and is associated with a first-order QPT [3,4]. Evidence of a second-order QPT that occurs between spherical vibrational and γ-soft systems has also been found in several mass regions, and one of the best-studied cases are the Ba and Xe nuclei with mass $A \approx 130$. In particular, the isotope ^{134}Ba has been identified [5] as the first empirical realization of the E(5) critical-point symmetry [6] of a second-order QPT.

Numerous theoretical studies have explored, predicted, and described nuclear QPTs, based on the nuclear shell model [7,8], nuclear density functional theory [9,10], geometrical models [2], and algebraic approaches [2,11]. Most of these analyses, however, have only considered even-even nuclei. In these systems nucleons are coupled pairwise, and the low-energy excitation spectra are characterized by collective degrees of freedom [12,13]. A theoretical investigation of QPT in systems with odd Z and/or N can be much more complicated because one needs to consider both the collective (even-even core) as well as single-particle [unpaired nucleon(s)] degrees of freedom that determine low-energy excitations [13]. Important questions that must be addressed when considering QPTs in odd-A systems include the effect of the odd particle on the location and nature of a phase transition, and the identification and evaluation of quantum order parameters. QPTs in odd-mass systems currently present a very active research topic [14–16]. In the last few years a number of phenomenological methods have been developed to study QPTs in odd-A nuclei [14–19]. Microscopic approaches, however, have not been extensively applied to QPTs in these systems.

Recently we have developed a theoretical method [20] for odd-mass nuclei, that is based on nuclear density functional theory and the particle-vibration coupling scheme. In this approach the even-even core is described in the framework of the interacting boson model (IBM) [21] using s and d bosons, which correspond to collective pairs of valence nucleons with $J^\pi = 0^+$ and 2^+ [22], respectively, and for the particle-core coupling the interacting boson-fermion model (IBFM) [23] is used. The deformation energy surface of an even-even nucleus as a function of the quadrupole shape variables (β,γ), as well as the single-particle energies and occupation probabilities of the odd nucleons, are obtained in a self-consistent mean-field calculation for a specific choice of the nuclear energy density functional (EDF) and a pairing interaction, and they determine the microscopic input for the parameters of the IBFM Hamiltonian. Only the strength parameters of the boson-fermion coupling terms in the IBFM Hamiltonian have to be adjusted to low-energy data in the considered odd-A nucleus. In Ref. [24] this method has been applied to an analysis of the signatures of shape-phase transitions in the axially deformed odd-mass Eu and Sm isotopes, and several mean-field and spectroscopic properties have been identified as possible quantum order parameters of the phase transition.

The aim of this work is to extend the analysis of Ref. [24] to γ-soft odd-A systems. In the present study we consider odd-A Xe ($Z = 54$), Cs ($Z = 55$), Ba ($Z = 56$), and La ($Z = 57$) isotopes with mass $A \approx 130$. As mentioned above, the even-even nuclei of Ba and Xe in this mass region present an excellent example of a second-order QPT that occurs between nearly spherical and γ-soft equilibrium shapes [2]. The low-lying states of the corresponding odd-A nuclei are described in terms of the even-even cores Ba and Xe, coupled to an unpaired neutron (odd-A Ba and Xe) or proton (odd-A La and Cs). Similarly to our previous work on QPTs in odd-N (Sm) and odd-Z (Eu) nuclei [24], here we consider the two possible cases that arise in odd-A systems: (i) the unpaired nucleon (neutron) is of the same type as the control parameter (neutron number) of the corresponding even-even boson core nuclei (the case of odd-A Ba and Xe), and (ii) the unpaired nucleon (proton) is of different type from the control parameter (the case of odd-A La and Cs). In general, the boson-fermion interaction will not be the same in the two cases and, therefore, one expects a distinct effect on the shape-phase transition that characterizes the even-even boson core.

Section II contains a short outline of the theoretical method used in the present study. In Sec. III we analyze the deformation energy surfaces for the even-even Ba and Xe isotopes, and compare the calculated low-energy excitation spectra and electromagnetic properties of the odd-mass Ba, Xe, La, and Cs nuclei to available spectroscopic data. We also compute and examine quadrupole shape invariants as signatures of shape-phase transitions in odd-A γ-soft systems. A summary of the main results and a brief outlook for future studies are included in Sec. IV.

II. MODEL PARTICLE-CORE HAMILTONIAN

The IBFM Hamiltonian, used here to describe the structure of excitation spectra of odd-A nuclei, consists of three terms: the even-even boson-core IBM Hamiltonian $\hat{H}_B$, the single-particle Hamiltonian for the unpaired fermions $\hat{H}_F$, and the boson-fermion coupling Hamiltonian $\hat{H}_{BF}$.

$$\hat{H} = \hat{H}_B + \hat{H}_F + \hat{H}_{BF}. \tag{1}$$

The number of bosons N_B and fermions N_F are assumed to be conserved separately and, since in the present study we only consider low-energy excitation spectra, $N_F = 1$. The building blocks of the IBM framework are s and d bosons that represent collective pairs of valence nucleons coupled to angular momentum $J^\pi = 0^+$ and 2^+, respectively [22]. N_B equals the number of valence fermion pairs, and no distinction is made between proton and neutron bosons. We employ the following form for the IBM Hamiltonian $\hat{H}_B$:

$$\hat{H}_B = \epsilon_d \hat{n}_d + \kappa \hat{Q}_B \cdot \hat{Q}_B, \tag{2}$$

with the d-boson number operator $\hat{n}_d = d^\dagger \cdot \tilde{d}$, and the quadrupole operator $\hat{Q}_B = s^\dagger \tilde{d} + d^\dagger \tilde{s} + \chi [d^\dagger \times \tilde{d}]^{(2)}$. ϵ_d, κ, and χ are strength parameters. The single-fermion Hamiltonian reads $\hat{H}_F = \sum_j \epsilon_j [a_j^\dagger \times \tilde{a}_j]^{(0)}$, where $a_j^\dagger$ and a_j are the fermion creation and annihilation operators, respectively, and ϵ_j denotes the single-particle energy of the orbital j. For the boson-fermion coupling Hamiltonian $\hat{H}_{BF}$ we use [23]:

$$\begin{aligned}\hat{H}_{BF} = & \sum_{jj'} \Gamma_{jj'} \hat{Q}_B \cdot [a_j^\dagger \times \tilde{a}_{j'}]^{(2)} \\ & + \sum_{jj'j''} \Lambda_{jj'}^{j''} : [[d^\dagger \times \tilde{a}_j]^{(j'')} \times [a_{j'}^\dagger \times \tilde{d}]^{(j'')}]^{(0)} : \\ & + \sum_j A_j [a^\dagger \times \tilde{a}_j]^{(0)} \hat{n}_d, \end{aligned} \tag{3}$$

where the first and second terms are referred to as the quadrupole dynamical and exchange interactions, respectively. The third term represents a monopole boson-fermion interaction. The strength parameters $\Gamma_{jj'}$, $\Lambda_{jj'}^{j''}$, and A_j can be expressed, by use of the generalized seniority scheme, in the following j-dependent forms [25]:

$$\Gamma_{jj'} = \Gamma_0 \gamma_{jj'} \tag{4}$$

$$\Lambda_{jj'}^{j''} = -2\Lambda_0 \sqrt{\frac{5}{2j''+1}} \beta_{jj''} \beta_{j'j''} \tag{5}$$

$$A_j = -A_0 \sqrt{2j+1}, \tag{6}$$

where $\gamma_{jj'} = (u_j u_{j'} - v_j v_{j'}) Q_{jj'}$ and $\beta_{jj'} = (u_j v_{j'} + v_j u_{j'}) Q_{jj'}$, with the matrix element of the quadrupole operator in the single-particle basis $Q_{jj'} = \langle j || Y^{(2)} || j' \rangle$. The factors u_j and v_j denote the occupation amplitudes of the orbit j, and satisfy the relation $u_j^2 + v_j^2 = 1$. Γ_0, Λ_0, and A_0 are strength parameters that have to be adjusted to low-energy structure data. A more detailed description of the model, and a discussion of various approximations, can be found in Ref. [20].

The first step in the construction of the IBFM Hamiltonian Eq. (1) are the parameters of the boson-core IBM term $\hat{H}_B$ that are determined using the mapping procedure developed in Refs. [26–28]: the (β,γ)-deformation energy surface, obtained in a constrained self-consistent mean-field calculation that also includes pairing correlations, is mapped onto the expectation value of $\hat{H}_B$ in the boson condensate state [29]. This procedure fixes the values of the parameters ϵ_d, κ, and χ of the boson Hamiltonian $\hat{H}_B$. As in our two previous studies of Refs. [20] and [24], the deformation energy surfaces of even-even Ba and Xe isotopes are calculated using the relativistic Hartree-Bogoliubov model based on the energy density functional DD-PC1 [30], and a separable pairing force of finite range [31]. The corresponding parameters of the IBM Hamiltonian for the isotopes $^{128-136}$Ba and $^{126-134}$Xe are listed in Table I.

For the fermion valence space we include all the spherical single-particle orbitals in the proton (neutron) major shell $Z(N) = 50$–82 for the odd-A La and Cs (Ba and Xe) isotopes: $3s_{1/2}$, $2d_{3/2}$, $2d_{5/2}$, and $1g_{7/2}$ for positive-parity states, and $1h_{11/2}$ for negative-parity states. Consistent with the definition of the IBFM Hamiltonian, the spherical single-particle energies ϵ_j and the occupation probabilities v_j^2 are obtained from the RHB model. The same RHB model calculation that determines the entire (β,γ)-deformation energy surface, when performed at zero deformation and with either the proton or neutron number constrained to the desired odd number,

TABLE I. Parameters of the boson Hamiltonian $\hat{H}_B$ (ϵ_d, κ, and χ) for $^{128-136}$Ba and $^{126-134}$Xe. The values of ϵ_d and κ are in units of MeV, while χ is dimensionless.

	ϵ_d	κ	χ
^{128}Ba	0.03	−0.102	−0.18
^{130}Ba	0.06	−0.116	−0.18
^{132}Ba	0.13	−0.122	−0.18
^{134}Ba	0.38	−0.124	−0.24
^{136}Ba	1.15	−0.122	−0.85
^{126}Xe	0.13	−0.115	−0.16
^{128}Xe	0.06	−0.132	−0.18
^{130}Xe	0.07	−0.142	−0.18
^{132}Xe	0.3	−0.144	−0.52
^{134}Xe	0.65	−0.144	−0.88

but without blocking, gives the canonical single-particle energies and occupation probabilities of the odd-fermion orbitals included in Tables II and III, respectively. Note that the exchange boson-fermion interaction in Eq. (3) takes into account the fact that the bosons are fermion pairs.

Finally, the three strength constants of the boson-fermion interaction $\hat{H}_{BF}$ ($\Gamma_0^{\pm}$, $\Lambda_0^{\pm}$, and $A_0^{\pm}$) are the only phenomenological parameters and, for each nucleus, their values are adjusted to reproduce a few lowest experimental states, separately for positive- and negative-parity states [20].

In Table IV we display the fitted strength parameters of $\hat{H}_{BF}$ for the positive-parity states. The strength of the quadrupole dynamical term Γ_0^+ is almost constant for each isotopic chain, except for the heaviest isotopes near the closed shell at $N = 82$, whose structure differs significantly from the lighter ones.

TABLE II. Spherical single-particle energies for the $2d_{3/2}$, $2d_{5/2}$, and $1g_{7/2}$ orbitals (in MeV) relative to that of the $3s_{1/2}$ orbital, obtained in the RHB calculation for the odd-mass nuclei considered in the present study.

	$2d_{3/2}$	$2d_{5/2}$	$1g_{7/2}$
^{129}Ba	0.410	2.528	4.619
^{131}Ba	0.455	2.574	4.761
^{133}Ba	0.498	2.619	4.898
^{135}Ba	0.539	2.665	5.030
^{137}Ba	0.578	2.714	5.157
^{127}Xe	0.358	2.530	4.326
^{129}Xe	0.400	2.582	4.450
^{131}Xe	0.433	2.625	4.562
^{133}Xe	0.479	2.682	4.684
^{135}Xe	0.516	2.733	4.795
^{129}La	−0.689	−2.726	−4.538
^{131}La	−0.737	−2.752	−4.716
^{133}La	−0.780	−2.772	−4.896
^{135}La	−0.814	−2.785	−5.073
^{137}La	−0.837	−2.788	−5.239
^{127}Cs	−0.704	−2.798	−4.467
^{129}Cs	−0.745	−2.822	−4.642
^{131}Cs	−0.781	−2.840	−4.824
^{133}Cs	−0.814	−2.853	−5.010
^{135}Cs	−0.844	−2.863	−5.199

TABLE III. Occupation probabilities of the spherical single-particle orbitals obtained in the SCMF calculation for the odd-A isotopes.

	$3s_{1/2}$	$2d_{3/2}$	$2d_{5/2}$	$1g_{7/2}$	$1h_{11/2}$
^{129}Ba	0.597	0.708	0.938	0.974	0.453
^{131}Ba	0.682	0.785	0.953	0.979	0.568
^{133}Ba	0.768	0.854	0.967	0.985	0.687
^{135}Ba	0.856	0.916	0.980	0.991	0.810
^{137}Ba	0.950	0.973	0.993	0.997	0.936
^{127}Xe	0.650	0.738	0.945	0.973	0.431
^{129}Xe	0.736	0.812	0.958	0.979	0.547
^{131}Xe	0.818	0.875	0.971	0.985	0.670
^{133}Xe	0.894	0.929	0.983	0.991	0.798
^{135}Xe	0.966	0.978	0.994	0.997	0.931
^{129}La	0.016	0.033	0.154	0.718	0.023
^{131}La	0.014	0.029	0.132	0.739	0.022
^{133}La	0.012	0.025	0.110	0.759	0.020
^{135}La	0.010	0.022	0.089	0.779	0.018
^{137}La	0.008	0.018	0.070	0.797	0.017
^{127}Cs	0.011	0.023	0.091	0.534	0.017
^{129}Cs	0.010	0.020	0.078	0.546	0.017
^{131}Cs	0.009	0.018	0.065	0.558	0.016
^{133}Cs	0.008	0.016	0.053	0.569	0.015
^{135}Cs	0.007	0.014	0.044	0.578	0.014

The strength parameter of the exchange term $\Lambda_0{}^+$ exhibits a gradual variation (either increase or decrease) with neutron number. While in the phenomenological IBFM calculations [32,33] a j-independent monopole strength was used for all fermion orbitals, in the present analysis, as in our previous study of Ref. [20], the strength parameter of the monopole interaction is allowed to be j dependent, $A_0 \equiv A'_j$ for positive-

TABLE IV. Parameters of the boson-fermion Hamiltonian $\hat{H}_{BF}$ for positive-parity states. All entries are in units of MeV.

	Γ_0^+	Λ_0^+	$A'_{1/2}$	$A'_{3/2}$	$A'_{5/2}$	$A'_{7/2}$
^{129}Ba	0.6	5.0	−0.21			−0.88
^{131}Ba	0.6	3.5	−0.09			
^{133}Ba	0.6	3.5		−0.05		
^{135}Ba	0.6	2.0		−0.55		
^{137}Ba	2.0	1.0		−1.3		
^{127}Xe	0.6	4.0	−0.28			−0.92
^{129}Xe	0.6	2.5	−0.12			−1.01
^{131}Xe	0.4	2.0		−0.27		
^{133}Xe	1.5	1.0		−0.95		
^{135}Xe	2.0	1.0		−1.35		
^{129}La	0.2	1.15			−1.20	
^{131}La	0.2	1.25			−1.25	
^{133}La	0.2	1.5			−0.82	
^{135}La	0.2	2.2			−1.11	
^{137}La	0.01	3.0			−1.5	
^{127}Cs	0.4	2.2			−1.5	
^{129}Cs	0.4	1.85			−1.5	
^{131}Cs	0.4	1.0			−0.7	
^{133}Cs	0.2	1.3			−1.05	
^{135}Cs	0.2	1.3			−1.35	

TABLE V. Same as in the caption to Table IV, but for negative-parity states.

	Γ_0^-	Λ_0^-	$A'_{11/2}$
^{129}Ba	0.6	2.1	−0.15
^{131}Ba	0.6	2.1	−0.23
^{133}Ba	0.6	0.9	0.0
^{135}Ba	0.6	1.0	−0.9
^{137}Ba	0.4	5.0	−0.6
^{127}Xe	0.6	2.0	−0.2
^{129}Xe	0.6	1.7	−0.13
^{131}Xe	0.6	1.6	−0.10
^{133}Xe	0.4	1.0	−0.20
^{135}Xe	0.45	0.0	0.0
^{129}La	0.1	0.0	−0.3
^{131}La	0.1	0.0	−0.28
^{133}La	0.1	0.0	0.0
^{135}La	0.1	0.0	0.0
^{137}La	0.1	10.0	−0.2
^{127}Cs	0.1	0.0	−0.07
^{129}Cs	0.1	0.0	−0.11
^{131}Cs	0.1	0.0	−0.05
^{133}Cs	0.6	0.0	−0.20

parity states. This is because the microscopic single-particle energies that we use in the present calculation are rather different from the empirical ones employed in Refs. [32,33]. In the case of ^{135}Ba, for instance, the single-particle orbital $2d_{3/2}$ is here calculated ≈0.5 MeV above the $3s_{1/2}$ orbital. In the fully phenomenological model of Ref. [33], on the other hand, the ordering of the two orbitals is reversed, that is, $\epsilon_{d_{3/2}} < \epsilon_{s_{1/2}}$. This is consistent with the empirical interpretation that the lowest and second-lowest positive-parity states of ^{135}Ba, with $J^\pi = 3/2_1{}^+$ and $1/2_1{}^+$, are predominantly based on the $2d_{3/2}$ and $3s_{1/2}$ configurations, respectively. To reproduce the correct empirical level ordering of the lowest two positive-parity states of ^{135}Ba, here the monopole term is adjusted specifically for the $2d_{3/2}$ orbital so that the $J^\pi = 3/2_1{}^+$ state becomes the lowest positive-parity state. We have also verified that with an j-independent monopole strength the empirical low-lying positive-parity spectra of ^{135}Ba cannot be reproduced.

For the negative-parity states (Table V), the three strength parameters (Γ_0^-, Λ_0^-, and A_0^-) are either constant or change gradually with neutron number. Since the exchange term gives only a small contribution for the negative-parity spectra of the odd-Z (La and Cs) isotopes, the exchange interaction strength $\Lambda_0{}^-$ is set to zero.

The resulting IBFM Hamiltonian $\hat{H}$ is diagonalized in the spherical basis $|j,L,\alpha,J\rangle$ using the code PBOS [34], where $\alpha = (n_d,v,n_\Delta)$ is a generic notation for the boson quantum numbers in the U(5) symmetry limit [21], which distinguish states with the same angular momentum of the boson system L. J is the total angular momentum of the coupled boson-fermion system, and satisfies the condition $|L - j| \leqslant J \leqslant L + j$.

By using the corresponding eigenfunctions, electromagnetic decay properties, such as $E2$ and $M1$ transition rates, and spectroscopic quadrupole and magnetic moments, are calculated for the odd-mass systems. The $E2$ operator contains the boson and fermion terms $\hat{T}^{(E2)} = \hat{T}_B^{(E2)} + \hat{T}_F^{(E2)}$. The expression for the IBM boson $E2$ operator:

$$\hat{T}_B^{(E2)} = e_B(s^\dagger\tilde{d} + d^\dagger\tilde{s} + \chi'[d^\dagger \times \tilde{d}]^{(2)}), \tag{7}$$

where e_B is the boson effective charge and χ' is a parameter. The fermion $E2$ operator used in the present calculation reads:

$$\hat{T}^{(E2)} = -e_F \sum_{jj'} \frac{1}{\sqrt{5}}\gamma_{jj'}[a^\dagger \times \tilde{a}_{j'}]^{(2)}, \tag{8}$$

with the fermion effective charge e_F. As in many phenomenological studies and also in our previous articles on shape-phase transitions in odd-A nuclei [20,24], the effective charge e_B is determined by the experimental value of $B(E2; 2_1{}^+ \rightarrow 0_1{}^+)$ in each even-even core nucleus. The parameter χ' is adjusted to reproduce the experimental spectroscopic quadrupole moment of the $2_1{}^+$ state (denoted as $Q_{2_1{}^+}$) of ^{136}Ba, and is fixed to the value $\chi' = 0.35$ for all nuclei considered in the present study. Finally, the value of the fermion effective charges e_F are adjusted to the experimental values of $Q_{5/2_1{}^+}$ of ^{137}La and $Q_{11/2_1{}^-}$ of ^{137}Ba. The corresponding proton $e_p = 0.250\,e$b and neutron $e_n = 0.125\,e$b effective charges are used for the odd-Z nuclei and odd-N nuclei, respectively. These values are consistent with standard IBFM calculations performed in this and other mass regions [33,35–37], as well as with the microscopic analysis of the IBFM [38]. The $M1$ operator is given by

$$\hat{T}^{(M1)} = \sqrt{\frac{3}{4\pi}}\left(\hat{T}_B^{(M1)} + \hat{T}_F^{(M1)}\right) \tag{9}$$

where $\hat{T}_B^{(M1)} = g_B\hat{L}$ is the boson $M1$ operator, and the fermion operator $\hat{T}_F^{(M1)}$ [25]:

$$\hat{T}_F^{(M1)} = -\sum_{jj'} g_{jj'}\sqrt{\frac{j(j+1)(2j+1)}{3}}[a_j^\dagger \times \tilde{a}_{j'}]^{(1)}, \tag{10}$$

with

$$g_{jj'} = \begin{cases} \frac{(2j-1)g_l+g_s}{2j} & (j = j' = l + \frac{1}{2}) \\ \frac{(2j+3)g_l-g_s}{2(j+1)} & (j = j' = l - \frac{1}{2}) \\ (g_l - g_s)\sqrt{\frac{2l(l+1)}{j(j+1)(2j+1)(2l+1)}} & (j' = j-1; l = l') \end{cases}, \tag{11}$$

and l is the orbital angular momentum of the single-particle state. The value of the boson g factor is $g_B = \mu_{2_1{}^+}/2$, where $\mu_{2_1{}^+}$ is the magnetic moment of the state $2_1{}^+$ of the even-even nucleus, and the corresponding experimental value is used for this quantity. For the fermion g factors: $g_l = 1.0\,\mu_N^2$ for the odd proton, and $g_l = 0$ for the odd neutron, and free values of g_s are quenched by 30% as used, for instance, in Refs. [20,38].

Summarizing this section, we note that the IBFM Hamiltonian (1) in the present implementation contains altogether 22 parameters. While the parameters of the boson and fermion Hamiltonians are determined by the microscopic self-consistent mean-field calculation, nine parameters: $\Gamma_0{}^\pm$, $\Lambda_0{}^\pm$, and A'_j for five orbitals, are specifically adjusted to experimental low-energy excitation spectra. In addition, the four

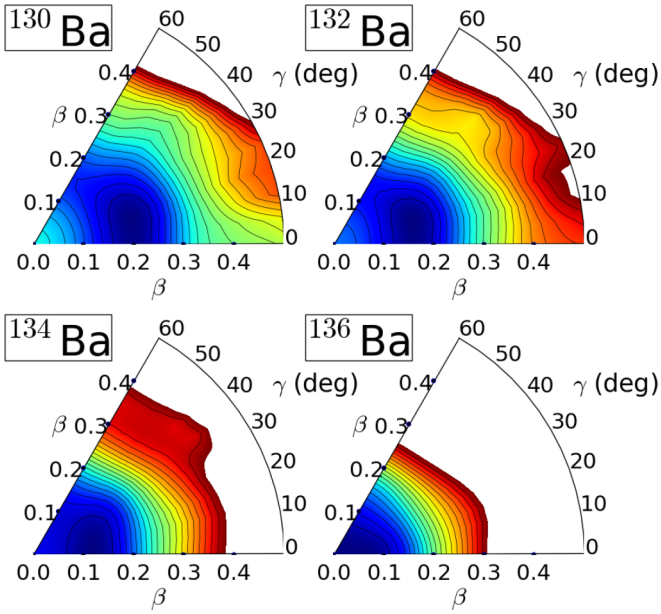

FIG. 1. Self-consistent RHB triaxial quadrupole binding energy maps of the even-even $^{130-136}$Ba isotopes in the β-γ plane ($0 \leqslant \gamma \leqslant 60^{\circ}$). For each nucleus the energy surface is normalized with respect to the binding energy of the absolute minimum, and is plotted up to 10 MeV excitation energy with 0.2 MeV difference between neighboring contours.

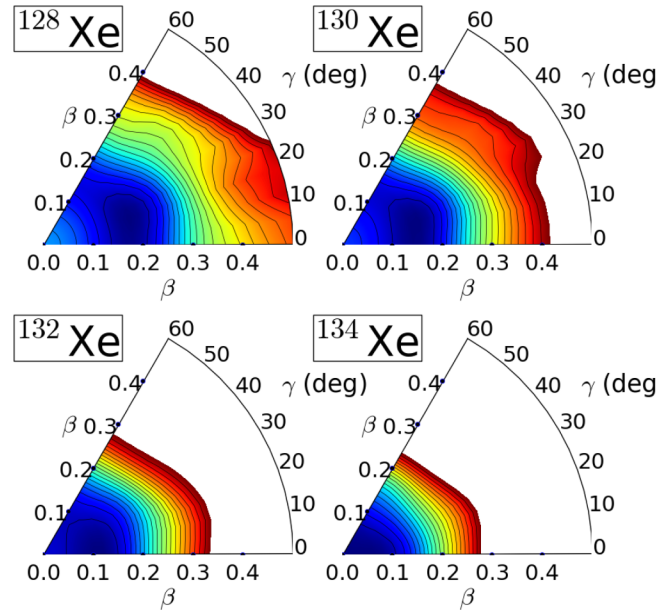

FIG. 2. Same as in the caption to Fig. 2, but for $^{128-134}$Xe.

parameters e_B, χ', e_p, and e_n of the $E2$ operator, are adjusted to reproduce specific $E2$ data.

III. SIGNATURES OF SHAPE-PHASE TRANSITIONS IN THE ODD-A γ-SOFT NUCLEI

A. Deformation energy surface

As explained in the previous section, the deformation energy surfaces for a set of even-even Ba and Xe isotopes that determine the parameters of the IBM Hamiltonian, are calculated as functions of the polar deformation parameters β and γ [12], using the constrained relativistic Hartree-Bogoliubov method based on the functional DD-PC1 [30] and a separable pairing force of finite range [31]. A triaxial binding energy map as a function of quadrupole shape variables is obtained by imposing constraints on both the axial and triaxial mass quadrupole moments. In Figs. 1 and 2, the energy surfaces for the even-even core nuclei $^{130-136}$Ba and $^{128-134}$Xe, respectively, are displayed in the β-γ plane ($0^{\circ} \leqslant \gamma \leqslant 60^{\circ}$). We note that the energy surfaces for the ^{128}Ba and ^{126}Xe nuclei are nearly identical to those of their adjacent nuclei ^{130}Ba and ^{128}Xe, respectively, and thus are not included in the figures.

At the self-consistent mean-field level the RHB energy surfaces display a gradual transition of equilibrium shapes as a function of the (valence) neutron number. One notices that the RHB energy surfaces for the Ba and Xe isotopes are very similar and, for this reason, we discuss only the results for the Ba isotopes. As shown in Fig. 1, the shape is noticeably soft in γ deformation for ^{130,132}Ba with a very shallow triaxial minimum in the interval $\gamma = 10^{\circ}$–20°. As the number of valence nucleons (neutron holes) decreases for ^{134}Ba, the potential appears to become almost completely flat in the γ direction, which is a typical feature of transitional nuclei. ^{136}Ba displays a nearly spherical shape with a minimum at $\beta \approx 0.1$, reflecting the $N = 82$ neutron shell closure. It is interesting that the equilibrium shapes for the Ba nuclei display no significant change in the axial deformation β as a function of the neutron number. We also note that the RHB energy surfaces for the Xe isotopes appear to be somewhat softer in γ when compared to the corresponding Ba neighbors.

In the present analysis we are particularly interested in transitional nuclei. ^{134}Ba is located between the nearly spherical shapes close to $N = 82$ and the γ-soft shapes of lighter isotopes. This nucleus was analyzed as the first empirical realization [5] of the critical point of second-order QPT between spherical and γ-soft shapes, described by the E(5) symmetry [6]. This symmetry corresponds to the five-dimensional collective Hamiltonian (the intrinsic variables β and γ and the three Euler angles), with an infinite square-well potential in the axial deformation β, and independent of γ [6]. One notices that the microscopic deformation energy surface of ^{134}Ba in the present calculation is closest to the E(5)-like potential: it is flat bottomed for small values of the axial deformation $\beta < 0.2$, and almost completely flat in the γ direction. A similar shape is predicted for ^{132}Xe.

B. Low-energy excitation spectra

A QPT is characterized by a significant variation of order parameters as functions of the physical control parameter. While the analysis of potential energy surfaces provides an approximate indication of QPT at the mean-field level, the intrinsic deformation parameters are not observables and a quantitative analysis of the nuclear phase transitions must, therefore, extend beyond the simple Landau approach to include a direct calculation of observables that can be interpreted as quantum order parameters.

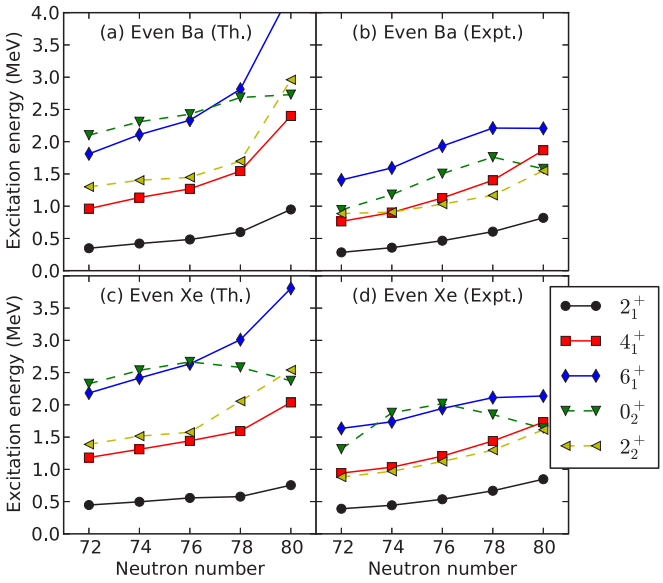

FIG. 3. Evolution of low-lying collective states in $^{128-136}$Ba and $^{126-134}$Xe, as functions of the neutron number. Theoretical excitation spectra in the left column are compared to data (panels on the right) from Ref. [39].

To illustrate the level of accuracy with which the boson-core Hamiltonian, with parameters determined by mapping the microscopic energy surface onto the expectation value of the IBM Hamiltonian, describes spectroscopic properties of even-even systems, we begin by comparing in Fig. 3 the computed excitation spectra for the low-lying states of the even-even $^{128-136}$Ba and $^{126-134}$Xe isotopes to available data [39]. Evidently the model calculation reproduces the empirical systematics of low-lying excitation spectra. In particular, the γ softness of the effective nuclear potential is characterized by close-lying 4_1^+ and 2_2^+ levels. Both experimentally and in model calculations, this level structure is observed from $N = 72$ up to 78. At $N = 80$ the energy spacings correspond to vibrational spectra, as identified by the multiplets of levels $(4_1^+, 2_2^+, 0_2^+)$. Overall, the theoretical excitation spectra are more stretched than the experimental ones, especially at $N = 80$. This could be attributed to the limited IBM configuration space consisting only of the valence nucleon pairs outside closed shells.

^{134}Ba is considered an excellent example of empirical realization of the E(5) critical-point symmetry [5]. In Fig. 4 we compare the calculated energy spectrum of this nucleus with the experimental low-energy levels, as well as with the spectrum corresponding to the E(5) symmetry limit. In comparison to the experimental levels, the present calculation generally predicts higher excitation energies, but exhibits several features that correspond to the E(5) symmetry, including the close-lying $(4_1^+, 2_2^+)$ and $(6_1^+, 4_2^+, 3_1^+, 0_2^+)$ levels, as well as the selection rule for $E2$ transitions from the 0_2^+ to the $2_{1,2}^+$ states.

In the following we focus the analysis on the results for odd-A systems. Figures 5–8 display the calculated low-energy positive ($\pi = +1$) and negative-parity ($\pi = -1$) levels of the odd-A isotopes $^{129-137}$Ba, $^{127-135}$Xe, $^{129-137}$La, and $^{127-135}$Cs,

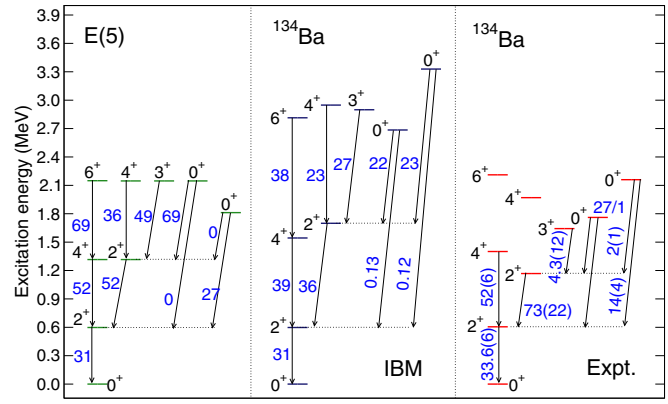

FIG. 4. The low-energy spectrum of ^{134}Ba calculated with the microscopic IBM, in comparison to available data [4,39]. The excitation spectrum that corresponds to the E(5) symmetry limit is also displayed, with the excitation energy of the state 2_1^+ and the $B(E2; 2_1^+ \rightarrow 0_1^+)$ transition strength normalized to the values obtained in the IBM calculation.

respectively, as functions of the neutron number, in comparison with the experimental excitation spectra [39]. We note a remarkable agreement between theory and experiment for both $\pi = +1$ and $\pi = -1$ states in all four isotopic chains.

A specific signature of QPT in odd-A nuclei is the change of the ground-state spin at a nucleon number that corresponds to the phase transition. For the odd-A Ba isotopes shown in Fig. 5, for instance, the spin of the lowest positive-parity state changes from $J^\pi = 1/2^+$ to $3/2^+$ at $N = 79$, while the change of the lowest negative-parity state from $J^\pi = 9/2^-$ to $11/2^-$ is observed at $N = 77$. This result is in agreement with the assumption that the QPT in the even-even Ba isotopes occurs at $N = 78$, that is, for ^{134}Ba. It also illustrates the difficulty in locating the point of shape-phase transition when the physical control parameter (neutron number in this case) is not continuous. One also notices in Figs. 5(a) and 5(b)

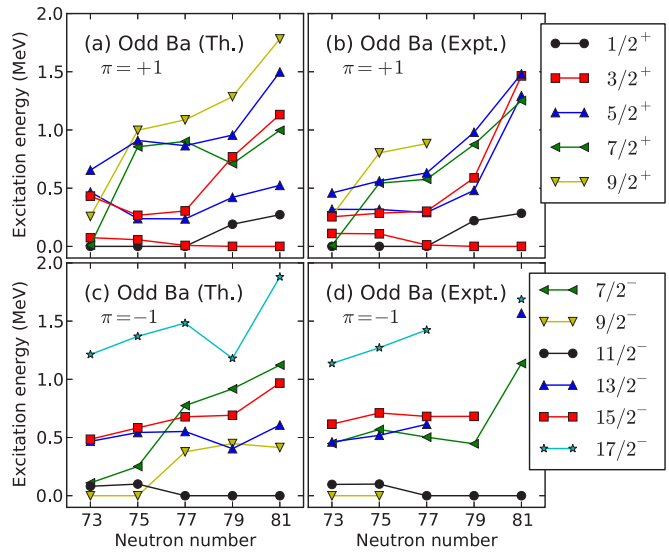

FIG. 5. Evolution of the low-lying positive- and negative-parity states in the odd-A isotopes $^{129-137}$Ba as functions of the neutron number. The experimental levels are from Ref. [39].

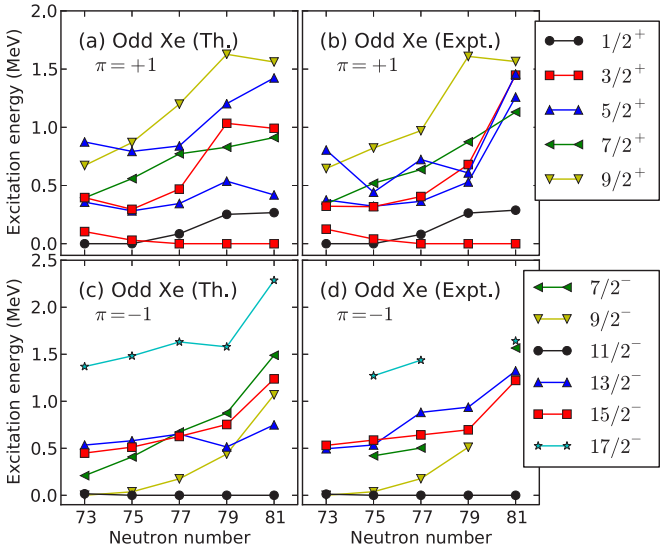

FIG. 6. Same as in the caption to Fig. 5, but for the isotopes $^{127-135}$Xe.

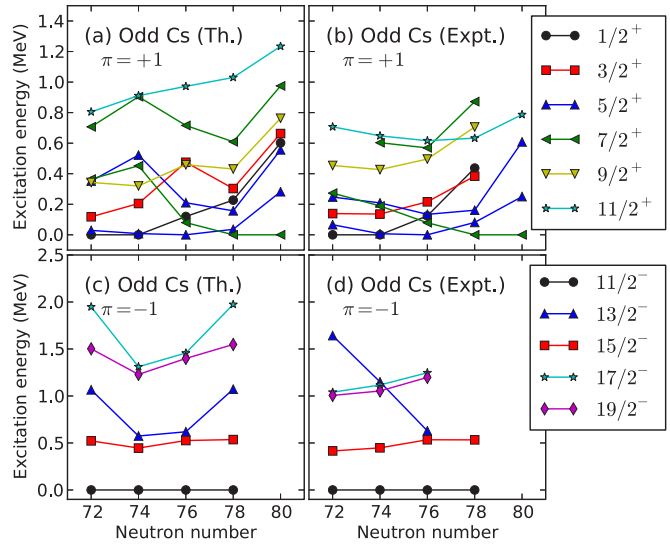

FIG. 8. Same as in the caption to Fig. 5, but for $^{127-135}$Cs.

that, compared to the other odd-A Ba isotopes considered, the $7/2_1{}^+$ and $9/2_1{}^+$ states at $N = 73$ are noticeably low in energy, almost degenerate with the $1/2_1{}^+$ ground state. Empirically, it has been suggested that these states predominantly correspond to the $1g_{7/2}$ configuration [32,39], reflecting the fact that the $1g_{7/2}$ single-particle orbital is particularly low at $N = 73$, and close in energy to the $3s_{1/2}$ and $2d_{3/2}$ orbitals. In our analysis, the calculated wave functions of the $7/2_1{}^+$ and $9/2_1{}^+$ states are almost pure (94 and 96%, respectively) $1g_{7/2}$ configurations, which conforms to the empirical interpretation of these states. Figure 6 displays a similar pattern for the odd-A Xe isotopes, except that in this case the change in spin of the lowest positive and negative parity states occurs already at $N = 77$ and $N = 75$, respectively.

In the odd-Z systems $^{129-137}$La (Fig. 7) and $^{127-135}$Cs (Fig. 8), on the one hand we notice the crossings between low-energy positive-parity levels in the transitional region between

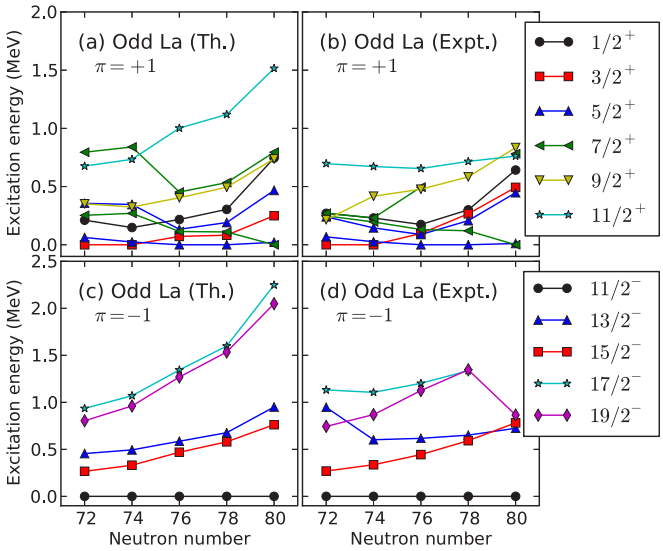

FIG. 7. Same as in the caption to Fig. 5, but for $^{129-137}$La.

$N = 76$ and $N = 78$. On the other hand, the negative-parity states of both odd-A La and Cs isotopes exhibit essentially the same level structure throughout the isotopic chains, that is, the band built on the $11/2^-$ state that follows the $\Delta J = 2$ systematics of the weak-coupling limit.

C. Detailed level schemes of selected odd-A nuclei

The details of the IBFM results are illustrated for one odd-A nucleus of each isotopic chain: ^{135}Ba, ^{129}Xe, ^{133}La, and ^{131}Cs. These specific nuclei are close to the shape-phase transition point, their low-energy level sequences are experimentally well established, and there is sufficient data to compare with model results, especially for the $E2$ and $M1$ transitions, as well as spectroscopic moments. Note that the calculated levels are classified into bands according to the dominant $E2$ decay branch.

^{135}Ba is of particular interest in the present analysis, since the corresponding even-even core ^{134}Ba can be, to a good approximation, characterized by the E(5) critical-point symmetry of the second-order QPT. In Ref. [40] the E(5/4) model of critical-point symmetry for odd-mass systems was developed, based on the concept of dynamical supersymmetry. The E(5/4) model describes the coupling of an unpaired $j = 3/2$ nucleon to the even-even boson core with E(5) symmetry. In fact, the first test of the E(5/4) Bose-Fermi symmetry [41] considered the low-energy spectrum of ^{135}Ba in terms of the neutron $2d_{3/2}$ orbital coupled to the E(5) boson core ^{134}Ba. In Fig. 9 we compare the IBFM low-energy positive-parity spectrum of ^{135}Ba and the corresponding $B(E2)$ values with the predictions of the E(5/4) model, as well as with the experimental excitation spectrum [41]. Evidently the E(5/4) spectrum is more regular, that is, it displays degenerate multiplets of excited states, when compared to both the present IBFM and experimental energy spectra. Moreover, the $E2$ branching ratios of the E(5/4) model, e.g., from the excited $3/2^+$ states, differ from those obtained in the present calculation. This is not surprising because E(5/4) presents a simple scheme that takes into

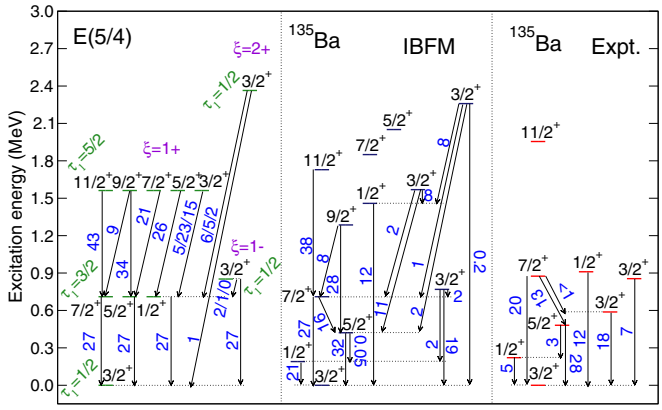

FIG. 9. The calculated low-energy positive-parity spectrum of ^{135}Ba (IBFM), compared to the corresponding experimental [41] and E(5/4) excitation spectra. The quantum numbers of the E(5/4) model are also shown. Note that the energy of the $(\xi = 1+, \tau_1 = 3/2)$ E(5/4) multiplet, i.e., $(7/2^+, 5/2^+, 1/2^+)$, is normalized to that of the $7/2_1{}^+$ IBFM state. $B(E2)$ values are given in Weisskopf units, and the $B(E2)$ from the $(\xi = 1+, \tau_1 = 3/2)$ E(5/4) multiplet is normalized to the $B(E2; 7/2_1{}^+ \rightarrow 3/2_1{}^+)$ value obtained in the present IBFM calculation. The triplets of $B(E2)$ values in the E(5/4) model spectrum refer to transitions to the $7/2_1{}^+$, $5/2_1{}^+$, and $1/2_1{}^+$ states, respectively.

account only a single neutron valence orbit $2d_{3/2}$. In the phenomenological IBFM calculation that was carried out in Ref. [41], the wave functions of the $1/2_1{}^+$ and $1/2_2{}^+$ states were found to be mainly composed of the $3s_{1/2}$ and $2d_{3/2}$ configurations, respectively, and it was thus suggested that the $1/2_1{}^+$ state in the first excited E(5/4) multiplet should be compared with the experimental $1/2_2{}^+$ state. Similar results are also obtained in the present calculation, as the $3s_{1/2}$ and $2d_{3/2}$ configurations account for 58% and 78% of the wave functions of the $1/2_1{}^+$ and $1/2_2{}^+$ states, respectively.

The present IBFM results reproduce the experimental excitation spectrum rather well, except for the fact that several non-yrast states, such as $1/2_2{}^+$, are calculated at higher excitation energies. In Table VI we also compare in detail the calculated $B(E2)$ and $B(M1)$ transition strengths, as well as the spectroscopic quadrupole (Q_J) and magnetic (μ_J) moments, with available data [39]. Considering the complexity of the level scheme and the large valence neutron space, a relatively good agreement is obtained between the calculated and experimental electromagnetic properties.

In Fig. 10 we display a detailed comparison between the IBFM theoretical and experimental [39] lowest-lying positive- and negative-parity bands of ^{129}Xe. For both parities the present calculation reproduces the structure of the experimental bands, especially the band-head energies. The low-energy positive- and negative-parity bands, both theoretical and experimental, exhibit a $\Delta J = 2$ systematics characteristic of the weak-coupling limit. The theoretical positive-parity bands are generally more stretched than the experimental ones, whereas a very good agreement between theory and experiment is obtained for the two negative-parity bands. Table VII compares the calculated and experimental $B(E2)$ and $B(M1)$ values, as well as the electromagnetic moments of ^{129}Xe.

TABLE VI. Comparison between the theoretical and experimental $B(E2)$ and $B(M1)$ values, and spectroscopic quadrupole and magnetic moments in ^{135}Ba. The data are from Ref. [39].

	$B(E2)$ (W.u.)		$B(M1)$ (W.u.)	
	Th.	Expt.	Th.	Expt.
$1/2_1{}^+ \rightarrow 3/2_1{}^+$	21	4.6(2)	0.0014	0.0025(11)
$1/2_2{}^+ \rightarrow 3/2_1{}^+$	12	11.7(10)	–	–
$3/2_2{}^+ \rightarrow 3/2_1{}^+$	2.0	18.0(10)	–	–
$3/2_3{}^+ \rightarrow 3/2_1{}^+$	4.6	7.0(10)	–	–
$5/2_1{}^+ \rightarrow 1/2_1{}^+$	0.05	2.6(5)	–	–
$5/2_1{}^+ \rightarrow 3/2_1{}^+$	32	28.3(10)	0.0012	0.0042(20)
$7/2_1{}^+ \rightarrow 3/2_1{}^+$	27	19.9(8)	–	–
$7/2_1{}^+ \rightarrow 5/2_1{}^+$	16	12.8(12)	0.0020	0.0032(3)
	Q_J (eb)		μ_J (μ_N^2)	
	Th.	Expt.	Th.	Expt.
$3/2_1{}^+$	+0.475	+0.160(3)	+0.769	+0.837943(17)
$11/2_1{}^-$	+1.13	+0.98(8)	−1.161	−1.001(15)

Next we consider the two odd-Z nuclei, for which the low-lying states predominantly correspond to the $1g_{7/2}$, $2d_{5/2}$ (positive-parity), and $1h_{11/2}$ (negative-parity) proton configurations. Figure 11 compares several calculated low-energy positive- and negative-parity bands of ^{133}La with available data. One notices a good agreement between the theoretical and experimental excitation spectra, except for that fact that some of the calculated bands, that is, the bands built on the $7/2_1{}^+$ state and the two negative-parity bands, appear more stretched than their experimental counterparts. Similar to ^{129}Xe, all the low-energy positive- and negative-parity bands shown here exhibit a $\Delta J = 2$ weak-coupling structure. The calculated and experimental $B(E2)$ and $B(M1)$ values, as well as the electromagnetic moments are listed in Table VIII.

The theoretical excitation spectrum of ^{131}Cs, shown in Fig. 12, is very similar to that of ^{133}La and, again, a very good agreement is obtained between the IBFM results and experiment. The calculated $E2$ and $M1$ transition strengths and electromagnetic moments are compared with the data [39]

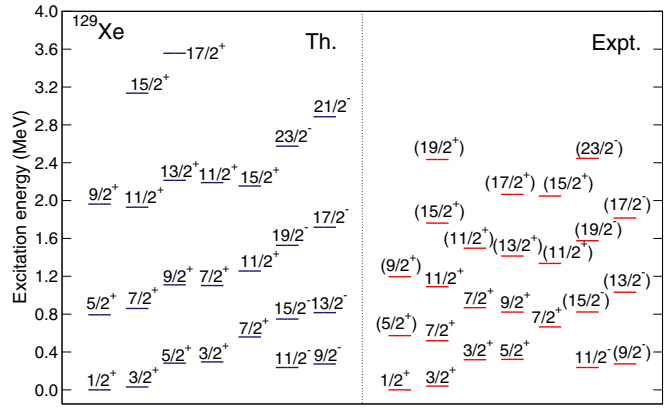

FIG. 10. Comparison between the IBFM theoretical and experimental [39] lowest-lying positive- and negative-parity bands of ^{129}Xe.

TABLE VII. Same as in the caption to Table VI, but for ^{129}Xe.

	$B(E2)$ (W.u.)		$B(M1)$ (W.u.)	
	Th.	Expt.	Th.	Expt.
$1/2_2^+ \to 1/2_1^+$	–	–	0.010	0.0016(5)
$1/2_2^+ \to 3/2_1^+$	22	6.7(23)	0.049	0.0039(13)
$1/2_2^+ \to 3/2_2^+$	–	–	0.0039	0.0015(5)
$1/2_2^+ \to 5/2_1^+$	0.018	1.4(6)	–	–
$3/2_1^+ \to 1/2_1^+$	0.89	9(4)	0.0019	0.0281(7)
$3/2_2^+ \to 1/2_1^+$	33	23^{+25}_{-23}	–	–
$3/2_2^+ \to 3/2_1^+$	16	17^{+27}_{-17}	0.00091	0.003^{+4}_{-3}
$3/2_3^+ \to 1/2_1^+$	7.4	>0.2	0.016	>0.0001
$3/2_3^+ \to 1/2_2^+$	8.1	>5.9	0.017	>0.0026
$3/2_3^+ \to 3/2_1^+$	9.2	>1.6	0.0027	>0.00071
$3/2_3^+ \to 3/2_2^+$	0.16	>3.4	0.029	>0.00037
$3/2_3^+ \to 5/2_1^+$	0.25	>4.6	0.00054	>0.0005
$5/2_1^+ \to 1/2_1^+$	13	21(4)	–	–
$5/2_1^+ \to 3/2_1^+$	46	5×10^{1}(4)	0.0013	0.011(5)
$5/2_4^+ \to 1/2_1^+$	2.0	15.4(19)	–	–
	Q_J (eb)		μ_J (μ_N^2)	
	Th.	Expt.	Th.	Expt.
$1/2_1^+$	–	–	−1.126	−0.7779763(84)
$3/2_1^+$	+0.362	−0.393(10)	+0.72	+0.58(8)
$11/2_1^-$	+0.092	+0.63(2)	−1.247	−0.891223(4)

in Table IX. We note that the model calculation qualitatively reproduces the complex transition pattern, but obviously the theoretical wave functions do not reflect the full extent of configuration mixing in this nucleus.

D. Effective β and γ deformations

Another signature of possible shape-phase transitions related to the γ softness of the effective nuclear potential, can be computed from $E2$ transition rates. Here we specifically analyze quadrupole shape invariants [42] (denoted hereafter as q invariants), calculated using $E2$ matrix elements. The lowest-order q invariants for a given state with spin J, relevant for the present study, are defined by the following

TABLE VIII. Same as in the caption to Table VI, but for ^{133}La.

	$B(E2)$ (W.u.)		$B(M1)$ (W.u.)	
	Th.	Expt.	Th.	Expt.
$1/2_1^+ \to 3/2_1^+$	9.4	6(3)	0.77	0.017(6)
$1/2_1^+ \to 5/2_1^+$	30	0.8(3)	–	–
$3/2_1^+ \to 5/2_1^+$	26	>35	0.13	>0.026
$5/2_2^+ \to 5/2_1^+$	15	2.1(10)	0.13	0.0097(8)
$7/2_1^+ \to 5/2_1^+$	18	11(4)	0.00011	0.0052(9)
$7/2_1^+ \to 5/2_2^+$	21	6.1(20)	1.0×10^{-5}	0.00068(16)
	Q_J (eb)		μ_J (μ_N^2)	
	Th.	Expt.	Th.	Expt.
$11/2_1^-$	–	–	+6.9	+7.5(4)

relations [43]:

$$q_2 = \sum_i^n \langle J||\hat{Q}||J_i'\rangle\langle J_i'||\hat{Q}||J\rangle \tag{12}$$

$$q_3 = \sqrt{\frac{7}{10}}\left|\sum_{i,j}^n \langle J||\hat{Q}||J_i'\rangle\langle J_i'||\hat{Q}||J_j'\rangle\langle J_j'||\hat{Q}||J\rangle\right|, \tag{13}$$

where $J' = J+2$, and the sum is in order of increasing excitation energies of the levels J'. Only a few lowest transitions contribute to the q invariants significantly and, in the present study, the sum runs up to $n = 5$. For even-even systems, we calculate the q invariants for the 0_1^+ ground state, which means $J = 0_1^+$ and $J' = 2^+$. The effective deformation parameters, denoted as $\beta_{\rm eff}$ and $\gamma_{\rm eff}$, can be obtained from q_2 and q_3 [43]:

$$\beta_{\rm eff} = \frac{4\pi}{3ZR_0^2}\sqrt{\frac{q_2}{2J'+1}}(J'2J0|JJ)^{-2} \tag{14}$$

$$\gamma_{\rm eff} = \frac{1}{3}\arccos\frac{q_3}{q_2^{3/2}}, \tag{15}$$

where $R_0 = 1.2A^{1/3}$ fm, and $(J'2J0|JJ)$ is the Clebsch-Gordan coefficient.

In Fig. 13 we plot $\beta_{\rm eff}$ and $\gamma_{\rm eff}$ for the even-even isotopes $^{128-136}$Ba and $^{126-134}$Xe, as functions of the neutron number.

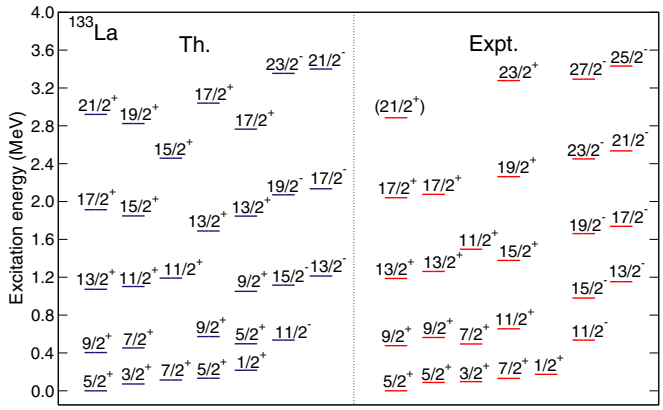

FIG. 11. Same as in the caption to Fig. 10, but for ^{133}La.

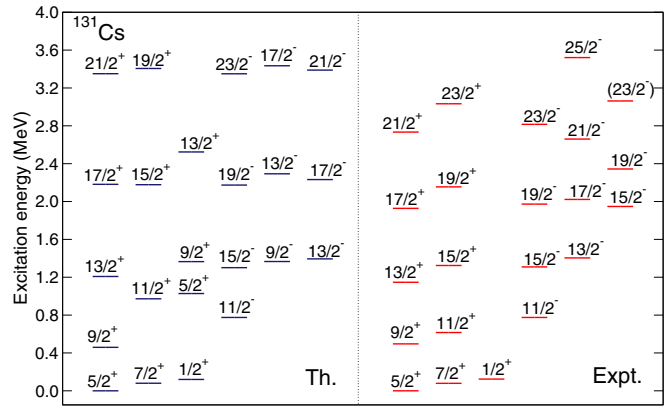

FIG. 12. Same as in the caption to Fig. 10, but for ^{131}Cs.

TABLE IX. Same as in the caption to Table VI, but for ^{131}Cs. Note that the sign is not known for the experimental $Q_{5/2_2^+}$ and $\mu_{11/2_1^-}$.

	$B(E2)$ (W.u.)		$B(M1)$ (W.u.)	
	Th.	Expt.	Th.	Expt.
$1/2_1^+ \to 5/2_1^+$	59	69.5(14)	–	–
$1/2_2^+ \to 1/2_1^+$	–	–	0.013	0.0010613(4)
$1/2_2^+ \to 3/2_1^+$	1.7	0.09(4)	0.011	3.4×10^{-5}(10)
$1/2_2^+ \to 3/2_2^+$	38	>0.62	0.0064	$>5.8 \times 10^{-5}$
$1/2_2^+ \to 5/2_1^+$	0.19	0.028248(4)	–	–
$1/2_2^+ \to 5/2_2^+$	4.7	0.13835(5)	–	–
$3/2_1^+ \to 1/2_1^+$	18	9(5)	0.30	0.00339(10)
$3/2_1^+ \to 5/2_1^+$	12	0.6(6)	0.22	0.00922(5)
$3/2_1^+ \to 5/2_2^+$	0.27	>3.9	0.0022	$>4.1^{-5}$
$3/2_1^+ \to 7/2_1^+$	1.4	2.36(3)	–	–
$3/2_2^+ \to 1/2_1^+$	0.94	2.4(4)	0.018	0.00057(4)
$3/2_2^+ \to 3/2_1^+$	0.012	>2.1	2.7×10^{-5}	$>7.8 \times 10^{-5}$
$3/2_2^+ \to 5/2_1^+$	0.55	2.4(9)	0.0012	0.00064(20)
$3/2_2^+ \to 5/2_2^+$	0.63	0.5(4)	0.0014	0.00071(4)
$3/2_2^+ \to 7/2_1^+$	25	0.2122(3)	–	–
$5/2_2^+ \to 5/2_1^+$	0.016	3.5(3)	0.0036	0.000369(17)
$5/2_2^+ \to 7/2_1^+$	45	>62	3.1×10^{-5}	$<2.1 \times 10^{-5}$
$7/2_1^+ \to 5/2_1^+$	0.10	0.64(24)	0.0010	0.00170(5)
	Q_J (eb)		μ_J (μ_N^2)	
	Th.	Expt.	Th.	Expt.
$5/2_1^+$	−0.772	−0.575(6)	+3.42	+3.543(2)
$5/2_2^+$	+0.370	0.022(2)	+0.37	+1.86(8)
$11/2_1^-$	–	–	+6.9	6.3(9)

One notices that, both for Ba and Xe nuclei, $\beta_{\rm eff}$ exhibits only a gradual decrease with neutron number. This correlates with the mean-field result, which indicates that the β deformation does not change significantly as a function of neutron number (cf. Figs. 1 and 2). In contrast, $\gamma_{\rm eff}$ displays a distinct peak at $N = 78$ for Ba and at $N = 76$ for Xe, which could be associated with the phase transition between nearly spherical and prominently γ-soft shapes. Indeed, the deformation energy surface at around these neutron numbers resembles the potential in the E(5) model, which is flat bottomed in an interval of the axial deformation β, and independent of γ.

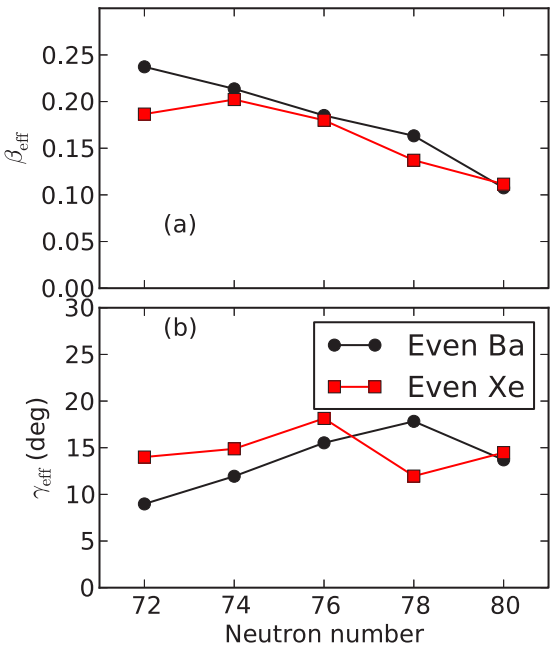

FIG. 13. $\beta_{\rm eff}$ and $\gamma_{\rm eff}$ for the 0_1^+ state of the even-even $^{128-136}$Ba and $^{126-134}$Xe isotopes, obtained from the computed q invariants.

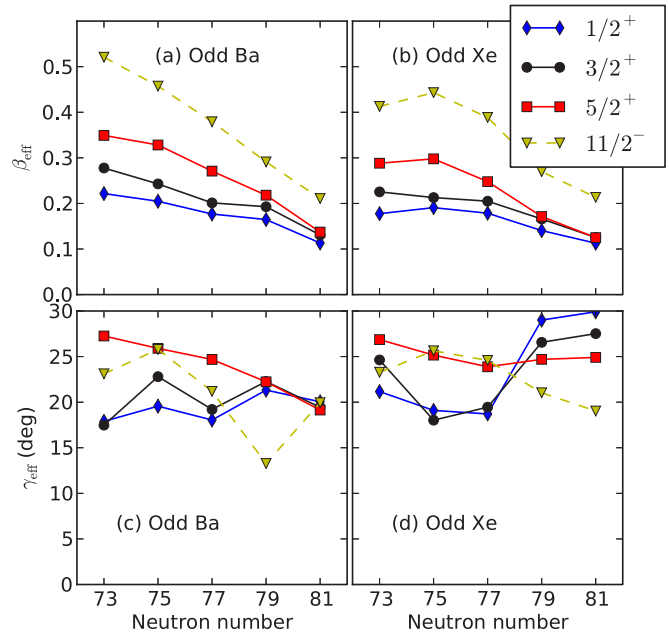

FIG. 14. Same as in the caption to Fig. 13, but for the $1/2_1^+$, $3/2_1^+$, $5/2_1^+$, and $11/2_1^-$ states of the odd-N $^{129-137}$Ba and $^{127-135}$Xe isotopes.

In the case of odd-A nuclei the spin of the ground state is not always the same for all isotopes, and we have thus calculated $\beta_{\rm eff}$ and $\gamma_{\rm eff}$ for several low-lying states. Figure 14 displays $\beta_{\rm eff}$ and $\gamma_{\rm eff}$ of the states $1/2_1^+$, $3/2_1^+$, $5/2_1^+$, and $11/2_1^-$ for the odd-N systems, that is, $^{129-137}$Ba and $^{127-135}$Xe. Similarly to the corresponding even-even core nuclei, in the odd-A Ba nuclei shown in Fig. 14(a) for all four states $\beta_{\rm eff}$ exhibits only a gradual decrease with the neutron number. For the states $5/2_1^+$ and $11/2_1^-$ in the odd-Xe nuclei, however, $\beta_{\rm eff}$ indicates a discontinuity at $N = 75$. $\gamma_{\rm eff}$, shown in Figs. 14(c) and 14(d), exhibits a significant change (either increase or decrease) for many states at $N = 79$. In addition, $\gamma_{\rm eff}$ for the states $3/2_1^+$ and $5/2_1^+$ of odd-A Ba nuclei displays another variation at $N = 75$. Similar results are also obtained for the odd-Z La and Cs nuclei, as shown in Fig. 15. However, $\gamma_{\rm eff}$ for the odd-Z La and Cs isotopes exhibits a more pronounced signature of shape-phase transition when compared to the odd-N Ba and Xe nuclei: a significant change at $N = 76$ or 78 for the odd-A La, and at $N = 76$ for the odd-A Cs isotopes.

IV. CONCLUDING REMARKS

Using the recently proposed method of Ref. [20], based on the microscopic framework of nuclear energy density functionals and the particle-core coupling scheme, we have analyzed signatures of QPTs in γ-soft odd-mass nuclei with

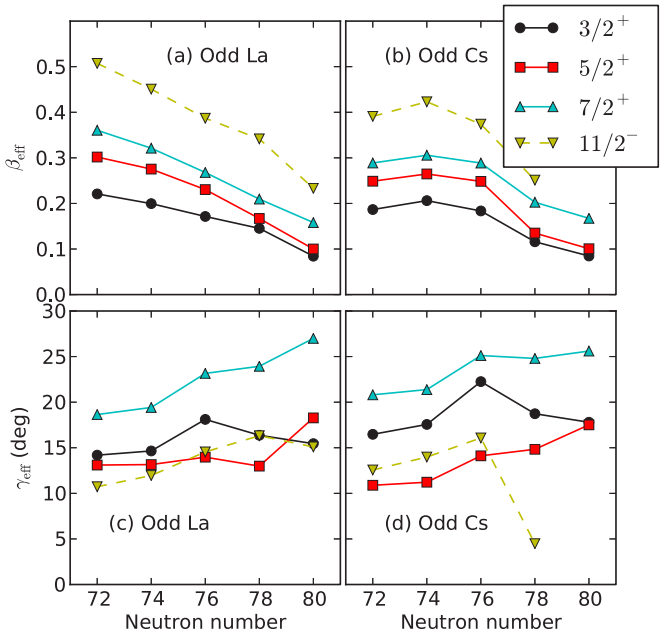

FIG. 15. Same as in the caption to Fig. 13, but for the $3/2_1{}^+$, $5/2_1{}^+$, $7/2_1{}^+$, and $11/2_1{}^-$ states of the odd-Z $^{129-137}$La and $^{127-135}$Cs isotopes.

mass $A \approx 130$. The deformation energy surface of the even-even core nuclei, and the spherical single-particle energies and occupation probabilities of the unpaired nucleon, are obtained by relativistic Hartree-Bogoliubov SCMF calculations with a specific choice of the energy density functional and pairing interaction.

The microscopic SCMF calculations determine the parameters of boson and fermion Hamiltonians used to model spectroscopic properties of the odd-A $^{129-137}$Ba, $^{127-135}$Xe, $^{129-137}$La, and $^{127-135}$Cs nuclei, whereas the strength parameters of the particle-core coupling are adjusted to reproduce selected empirical results of low-energy spectra in odd-A systems. The method provides a very good description of spectroscopic properties of the γ-soft odd-mass systems. Even though phase transitions are smoothed out in finite systems, especially a second-order QPT as the one considered here, and the physical control parameter takes only integer values (the nucleon number), the SCMF deformation energy surfaces and the resulting excitation spectra consistently point to a shape-phase transition in the interval $N = 76$–78, both in even-even and odd-mass systems. In particular, $\gamma_{\rm eff}$, evaluated using $E2$ matrix elements for transitions between low-lying states, clearly exhibits a discontinuity near $N = 76$ and 78, which signals the occurrence of a phase transition between nearly spherical and γ-soft shapes. The results obtained in this work, as well as in our previous studies on odd-A Sm and Eu [20,24], have shown that the method of Ref. [20] works not only in axially deformed nuclei, but also in γ-soft or axially asymmetric odd-mass systems, and enables a systematic investigation of the structural evolution in odd-A nuclei in medium-heavy and heavy-mass regions.

The necessity to fit the strength parameters of the boson-fermion coupling Hamiltonian to spectroscopic data in the considered odd-mass nuclei, presents a serious limitation of the current implementation of our IBF method. In contrast to the parameters of the boson and fermion Hamiltonians that are completely determined by the choice of a global EDF and pairing interaction, the boson-fermion coupling must be specifically adjusted for each odd-mass nucleus. This procedure, of course, limits the applicability to those nuclei for which enough low-energy structure data are available to completely determine the strength of the various boson-fermion interaction terms. Therefore, an important step forward would be to develop a method to microscopically determine, or at least constrain, the values of the boson-fermion coupling parameters. One possibility would be to perform SCMF calculations for odd-A systems and map the resulting deformation energy surface onto the expectation value of the IBFM Hamiltonian in the boson-fermion condensate state [44]. SCMF calculations for odd-A nuclei are, of course, computationally very challenging and such an approach would be difficult to apply in systematic studies of a large number of nuclei. Another strategy would be to derive the boson-fermion coupling from a microscopic shell-model interaction between nucleons in a given valence space [45]. In this approach the parameters can be determined by equating the matrix elements in the IBFM space to those in the shell-model space. The disadvantage of this method is that it requires the explicit introduction of a new building block, that is, the shell-model interaction. This is certainly an interesting problem and will be the topic of future studies and development of the semiphenomenological model employed in the present analysis.

ACKNOWLEDGMENTS

K.N. acknowledges support from the Japan Society for the Promotion of Science. This work has been supported in part by the Croatian Science Foundation, project "Structure and Dynamics of Exotic Femtosystems" (IP-2014-09-9159) and the QuantiXLie Centre of Excellence.

[1] *Understanding Quantum Phase Transitions*, edited by L. Carr (CRC Press, Boca Raton, 2010).
[2] P. Cejnar, J. Jolie, and R. F. Casten, Rev. Mod. Phys. **82**, 2155 (2010).
[3] F. Iachello, Phys. Rev. Lett. **87**, 052502 (2001).
[4] R. F. Casten and N. V. Zamfir, Phys. Rev. Lett. **87**, 052503 (2001).
[5] R. F. Casten and N. V. Zamfir, Phys. Rev. Lett. **85**, 3584 (2000).
[6] F. Iachello, Phys. Rev. Lett. **85**, 3580 (2000).
[7] N. Shimizu, T. Otsuka, T. Mizusaki, and M. Honma, Phys. Rev. Lett. **86**, 1171 (2001).
[8] T. Togashi, Y. Tsunoda, T. Otsuka, and N. Shimizu, Phys. Rev. Lett. **117**, 172502 (2016).

[9] T. Nikšić, D. Vretenar, G. A. Lalazissis, and P. Ring, Phys. Rev. Lett. **99**, 092502 (2007).
[10] Z. P. Li, T. Nikšić, D. Vretenar, and J. Meng, Phys. Rev. C **81**, 034316 (2010).
[11] P. Cejnar and J. Jolie, Prog. Part. Nucl. Phys. **62**, 210 (2009).
[12] A. Bohr and B. M. Mottelsson, *Nuclear Structure*, Vol. 2 (Benjamin, New York, 1975), p. 45.
[13] A. Bohr, Mat. Fys. Medd. Dan. Vid. Selsk. **27**, 16 (1953).
[14] F. Iachello, Riv. Nuovo Cimento **34**, 617 (2011).
[15] F. Iachello, A. Leviatan, and D. Petrellis, Phys. Lett. B **705**, 379 (2011).
[16] D. Petrellis, A. Leviatan, and F. Iachello, Ann. Phys. (N.Y.) **326**, 926 (2011).
[17] Y. Zhang, F. Pan, Y.-X. Liu, Y.-A. Luo, and J. P. Draayer, Phys. Rev. C **88**, 014304 (2013).
[18] Y. Zhang, L. Bao, X. Guan, F. Pan, and J. P. Draayer, Phys. Rev. C **88**, 064305 (2013).
[19] D. Bucurescu and N. V. Zamfir, Phys. Rev. C **95**, 014329 (2017).
[20] K. Nomura, T. Nikšić, and D. Vretenar, Phys. Rev. C **93**, 054305 (2016).
[21] F. Iachello and A. Arima, *The Interacting Boson Model* (Cambridge University Press, Cambridge, 1987).
[22] T. Otsuka, A. Arima, and F. Iachello, Nucl. Phys. A **309**, 1 (1978).
[23] F. Iachello and P. Van Isacker, *The Interacting Boson-Fermion Model* (Cambridge University Press, Cambridge, 1991).
[24] K. Nomura, T. Nikšić, and D. Vretenar, Phys. Rev. C **94**, 064310 (2016).
[25] O. Scholten, Prog. Part. Nucl. Phys. **14**, 189 (1985).
[26] K. Nomura, N. Shimizu, and T. Otsuka, Phys. Rev. Lett. **101**, 142501 (2008).
[27] K. Nomura, N. Shimizu, and T. Otsuka, Phys. Rev. C **81**, 044307 (2010).
[28] K. Nomura, T. Otsuka, N. Shimizu, and L. Guo, Phys. Rev. C **83**, 041302 (2011).
[29] J. N. Ginocchio and M. W. Kirson, Nucl. Phys. A **350**, 31 (1980).
[30] T. Nikšić, D. Vretenar, and P. Ring, Phys. Rev. C **78**, 034318 (2008).
[31] Y. Tian, Z. Y. Ma, and P. Ring, Phys. Lett. B **676**, 44 (2009).
[32] M. Cunningham, Nucl. Phys. A **385**, 221 (1982).
[33] F. Dellagiacoma, Ph.D. thesis, Yale University, 1988.
[34] T. Otsuka and N. Yoshida, Japan Atomic Energy Research Institute, Report No. 85, 1985.
[35] *Interacting Bose-Fermi Systems in Nuclei*, edited by F. Iachello (Springer, New York, 1981).
[36] N. Yoshida, H. Sagawa, T. Otsuka, and A. Arima, Nucl. Phys. A **503**, 90 (1989).
[37] S. Abu-Musleh, H. Abu-Zeid, and O. Scholten, Nucl. Phys. A **927**, 91 (2014).
[38] O. Scholten and N. Blasi, Nucl. Phys. A **380**, 509 (1982).
[39] Brookhaven National Nuclear Data Center, http://www.nndc.bnl.gov.
[40] F. Iachello, Phys. Rev. Lett. **95**, 052503 (2005).
[41] M. S. Fetea, R. B. Cakirli, R. F. Casten, D. D. Warner, E. A. McCutchan, D. A. Meyer, A. Heinz, H. Ai, G. Gürdal, J. Qian, and R. Winkler, Phys. Rev. C **73**, 051301 (2006).
[42] D. Cline, Annu. Rev. Nucl. Part. Sci. **36**, 683 (1986).
[43] V. Werner, N. Pietralla, P. von Brentano, R. F. Casten, and R. V. Jolos, Phys. Rev. C **61**, 021301 (2000).
[44] A. Leviatan, Phys. Lett. B **209**, 415 (1988).
[45] O. Scholten and A. E. L. Dieperink, in *Interacting Bose-Fermi Systems in Nuclei*, edited by F. Iachello (Springer, New York, 1981), p. 343.